Quantification of $CMRO_2$ without hypercapnia using simultaneous near-infrared spectroscopy and fMRI measurements

2010 Phys. Med. Biol. 55 3249

(http://iopscience.iop.org/0031-9155/55/11/017)

IOP PUBLISHING PHYSICS IN MEDICINE AND BIOLOGY

Phys. Med. Biol. **55** (2010) 3249–3269 doi:10.1088/0031-9155/55/11/017

Quantification of $CMRO_2$ without hypercapnia using simultaneous near-infrared spectroscopy and fMRI measurements

Sungho Tak, Jaeduck Jang, Kangjoo Lee and Jong Chul Ye[1]

Bio Imaging and Signal Processing Lab., Department of Bio and Brain Engineering, KAIST, 335 Gwahak-ro, Yuseong-gu, Daejeon 305-701, Korea

E-mail: jong.ye@kaist.ac.kr

Received 30 December 2009, in final form 26 February 2010
Published 17 May 2010
Online at stacks.iop.org/PMB/55/3249

Abstract

Estimation of the cerebral metabolic rate of oxygen ($CMRO_2$) and cerebral blood flow (CBF) is important to investigate the neurovascular coupling and physiological components in blood oxygenation level-dependent (BOLD) signals quantitatively. Although there are methods that can determine $CMRO_2$ changes using functional MRI (fMRI) or near-infrared spectroscopy (NIRS), current approaches require a separate hypercapnia calibration process and have the potential to incur bias in many assumed model parameters. In this paper, a novel method to estimate $CMRO_2$ without hypercapnia is described using simultaneous measurements of NIRS and fMRI. Specifically, an optimization framework is proposed that minimizes the differences between the two forms of the relative $CMRO_2$–CBF coupling ratio from BOLD and NIRS biophysical models, from which hypercapnia calibration and model parameters are readily estimated. Based on the new methods, we found that group average CBF, $CMRO_2$, cerebral blood volume (CBV), and BOLD changes within activation of the primary motor cortex during a finger tapping task increased by $39.5 \pm 21.4\%$, $18.4 \pm 8.7\%$, $12.9 \pm 6.7\%$, and $0.5 \pm 0.2\%$, respectively. The group average estimated flow-metabolism coupling ratio was 2.38 ± 0.65 and the hypercapnia parameter was $7.7 \pm 1.7\%$. These values are within the range of values reported from other literatures. Furthermore, the activation maps from CBF and $CMRO_2$ were well localized on the primary motor cortex, which is the main target region of the finger tapping task.

(Some figures in this article are in colour only in the electronic version)

[1] Author to whom any correspondence should be addressed.

0031-9155/10/113249+21$30.00

1. Introduction

Elucidating the underlying link between the changes in neuronal activity and the cerebral blood flow (CBF) or cerebral metabolic rate of oxygen ($CMRO_2$) has been of great interest in neuroimaging (Mukamel *et al* 2005, Schummers *et al* 2008, Gordon *et al* 2008, Smith *et al* 2002). The physiological background of neurovascular and neurometabolic coupling during brain activation is as follows: evoked neuronal activity induces dendrites to consume oxygen (O_2) rapidly (Kasischke *et al* 2004), which causes oxygen pressure (Ances *et al* 2001) to decrease (Malonek *et al* 1997). In the astrocyte, glycolysis is then enhanced (Kasischke *et al* 2004) and lactate is released (Hu and Wilson 2002). In response to the lactate, vasodilation occurs (Hein *et al* 2006). A summary of these processes is available in Gordon *et al* (2008). Fox and Raichle (1986) initially found that with somatosensory stimulation the increase in CBF (29%) exceeded a concurrent increase in $CMRO_2$ (5%). Numerous studies have confirmed that the fractional change in CBF is approximately minimum twice and maximum four times as large as the fractional change in $CMRO_2$ (Boas *et al* 2003, Hoge *et al* 1999a, 2005, Durduran *et al* 2004, Sheth *et al* 2004, Kastrup *et al* 2002, Kim *et al* 1999, Davis *et al* 1998). However, the physiological processes of flow-metabolism coupling during dynamic changes are still unresolved. Explaining the underlying mechanism of the flow-metabolism coupling is crucial for understanding the fundamental physiological effect of blood oxygenation level-dependent (BOLD) response. More specifically, the change in BOLD signal is caused by the combined effects of CBF, $CMRO_2$, and cerebral blood volume (CBV). To analyze the contributions of these components to BOLD response quantitatively, the balloon model (Buxton *et al* 1998b), the windkessel model (Mandeville *et al* 1999b), and the model formulated by Davis *et al* (1998) have been proposed. The main idea of the balloon model and the windkessel model is that the post-stimulus undershoot of the BOLD response is caused by a delay in the return to baseline by the CBV response, compared to CBF response. However, other studies have argued for a prolonged elevation of $CMRO_2$ (Frahm *et al* 2008, Lu *et al* 2004), and CBF undershoot in the presence of a slow venous CBV response (Chen and Pike 2009) as the primary contributor to BOLD undershoot. Therefore, to assess the main contributor of a transient BOLD response and investigate the neurovascular coupling in a quantitative manner, a robust estimation method of CBF and $CMRO_2$ is essential.

Determination of relative $CMRO_2$ changes using functional MRI (fMRI) has been traditionally obtained by measuring the CBF and BOLD changes (Davis *et al* 1998, Hoge *et al* 1999a, Kim *et al* 1999). Assuming that changes in $CMRO_2$ are negligible during hypercapnia (Horvath *et al* 1994), BOLD signals are calibrated against known changes in CBF. Relative $CMRO_2$ changes are then estimated from the relative changes of CBF and BOLD. While the fMRI approach of $CMRO_2$ estimation promises a high spatial resolution (Davis *et al* 1998, Uludağ *et al* 2004), there are several drawbacks. Most importantly, recent studies show that $CMRO_2$ continues to vary during CO_2 inhalation (Kliefoth *et al* 1979, Jones *et al* 2005, Sicard and Duong 2005), which challenges the important assumption of hypercapnia calibration, as inaccurate estimates of the hypercapnia calibration parameter lead to significant bias regarding the fractional CBF–$CMRO_2$ coupling ratio (Chiarelli *et al* 2007b). Although breath holding (Kastrup *et al* 1999) and hyperoxia calibration (Chiarelli *et al* 2007c) techniques have been introduced to overcome the disadvantages of the hypercapnia process, an additional measurement step is nonetheless required, which is inconvenient in that it may stress the subjects.

Near-infrared spectroscopy (NIRS) can also estimate changes in $CMRO_2$ from direct measurements of functional contrasts such as oxy-hemoglobin (HbO), deoxy-hemoglobin (HbR), and total-hemoglobin (HbT) (Boas *et al* 2003, Mayhew *et al* 2001a, 2001b,

Vignal *et al* 2008). Due to the high temporal resolution, the NIRS approach for $CMRO_2$ estimation has advantages over fMRI in that it is possible to characterize the transient response of $CMRO_2$ and CBF more accurately. However, current $CMRO_2$ estimation techniques based on NIRS measurements rely on multiple assumptions and depend considerably on baseline hemoglobin concentrations, which are difficult to measure through optical methods alone. Hoge *et al* (2005) proposed a method to determine relative $CMRO_2$ changes from the diffuse optical imaging and arterial spin labeling (ASL) techniques. The relative changes in $CMRO_2$ can be calculated as multiplying the relative oxygen extraction fraction and CBF, which are estimated from the optical and ASL measurements, respectively. While this approach does not require any relationship between CBF and CBV, uncertainties introduced by the assumptions of baseline hemoglobin concentration and the unknown partial volume difference between the MRI and optical measurements often limit the accuracy of this approach.

The main contribution of the present paper is to propose a novel method that estimates the changes in $CMRO_2$ and CBF with simultaneous NIRS and fMRI–BOLD measurements, in a manner that overcomes the limitations of earlier approaches. In the case of fMRI (Davis *et al* 1998), the relative coupling ratio between $CMRO_2$ and CBF can be represented as a nonlinear function of CBV and BOLD response. For NIRS (Mayhew *et al* 2001a, 2001b, Boas *et al* 2003), the relative coupling ratio between $CMRO_2$ and CBF arises from HbR and CBV in the venous compartment. Due to the simultaneous recording method, the relative coupling ratio separately derived from each modality should be identical. Therefore, by minimizing the difference between the coupling ratios from two biophysical models, the hypercapnia calibration parameter, the baseline hemoglobin concentrations, and other parameters can be accurately estimated without hypercapnia. Hence, the controversial assumption of $CMRO_2$ invariance during hypercapnia is not necessary in the proposed approach, which may enhance the reliability of this method in explaining the origin of BOLD.

2. Theory

2.1. Relative $CMRO_2$–CBF ratio from the BOLD biophysical model (Davis et al 1998, Hoge et al 1999a)

When the changes in the transverse relaxation rate caused by HbR, $\Delta R^*_{2,\mathrm{HbR}}(t)$, are small enough, the fractional changes in the T_2^*-weighted BOLD signals are approximated by

$$\begin{aligned}\frac{\Delta \mathrm{BOLD}(t)}{\mathrm{BOLD}_0} &\cong -\mathrm{TE}\Delta R^*_{2,\mathrm{HbR}}(t)\\ &\cong H\left(1-\mathrm{rCBV}(t)\left(\frac{[\mathrm{HbR}(t)]_v}{[\mathrm{HbR}]_{v_0}}\right)^{\beta}\right),\end{aligned} \tag{1}$$

where $\Delta R^*_{2,\mathrm{HbR}}(t) = c\big(\mathrm{CBV}(t)[\mathrm{HbR}(t)]_v^{\beta} - \mathrm{CBV}_0[\mathrm{HbR}]_{v_0}^{\beta}\big)$ (Boxerman *et al* 1995); the hypercapnia calibration parameter $H = \mathrm{TE}\cdot c\cdot \mathrm{CBV}_0[\mathrm{HbR}]_{v_0}^{\beta}$, where TE denotes the echo time, c denotes a constant dependent on the magnetic field strength and vascularity, and β is a constant that ranges from 1 to 2; $\mathrm{rCBV}(t)$ is the relative CBV to its baseline; $[\mathrm{HbR}(t)]_v = \mathrm{HbR}_v(t)/\mathrm{CBV}_v(t)$, $[\mathrm{HbR}]_{v0} = \mathrm{HbR}_{v0}/\mathrm{CBV}_{v0}$, where the subscript '0' denotes the baseline value, and the subscript 'v' denotes the venous vasculature, respectively.

Assuming that the HbR concentration in arterial blood is negligible, Fick's law gives the following relationship (Hoge *et al* 1999a):

$$\frac{[\mathrm{HbR}(t)]_v}{[\mathrm{HbR}]_{v0}} = \frac{\mathrm{rCMRO_2}(t)}{\mathrm{rCBF}(t)}, \tag{2}$$

where $\mathrm{rCMRO_2}(t)$ and $\mathrm{rCBF}(t)$ are relative $\mathrm{CMRO_2}$, and CBF to their respective baselines.

Substituting equation (2) for $[\mathrm{HbR}(t)]_v/[\mathrm{HbR}]_{v0}$ in equation (1), the relative $\mathrm{CMRO_2}$–CBF coupling ratio from the BOLD biophysical model is then derived as

$$\frac{\mathrm{rCMRO_2}(t)}{\mathrm{rCBF}(t)} = \mathrm{rCBV}(t)^{-1/\beta}\left(1 - \frac{1}{H}\cdot\frac{\Delta\mathrm{BOLD}(t)}{\mathrm{BOLD_0}}\right)^{1/\beta}. \tag{3}$$

2.2. Relative $\mathrm{CMRO_2}$–CBF ratio from the NIRS biophysical model (Boas et al 2003, Mayhew et al 2001a, 2001b)

Assuming that the quantities in the venous vasculature are proportional to those in the total vascular compartment (Mayhew *et al* 2001a, 2001b), the relative coupling ratio from the NIRS biophysical model is derived from Fick's law (Hoge *et al* 1999a) as

$$\begin{aligned}\frac{\mathrm{rCMRO_2}(t)}{\mathrm{rCBF}(t)} &= \frac{\mathrm{rHbR}_v(t)}{\mathrm{rCBV}_v(t)}\\ &= \frac{1+\gamma_r\,(\Delta\mathrm{HbR}(t)/\mathrm{HbR_0})}{1+\gamma_v\,(\Delta\mathrm{CBV}(t)/\mathrm{CBV_0})},\end{aligned} \tag{4}$$

where rHbR denotes relative HbR to its baseline, the venous HbR ratio γ_r and the venous HbT ratio γ_v are given by

$$\gamma_r = \frac{\Delta\mathrm{HbR}_v(t)/\mathrm{HbR}_{v0}}{\Delta\mathrm{HbR}(t)/\mathrm{HbR_0}} \qquad \gamma_v = \frac{\Delta\mathrm{CBV}_v(t)/\mathrm{CBV}_{v0}}{\Delta\mathrm{CBV}(t)/\mathrm{CBV_0}}. \tag{5}$$

2.3. Estimation of relative $\mathrm{CMRO_2}$–CBF coupling ratio without hypercapnia calibration

Substituting equation (2) into equation (1), the fractional changes in BOLD are given by

$$\frac{\Delta\mathrm{BOLD}(t)}{\mathrm{BOLD_0}} = H\left(1 - \mathrm{rCBV}(t)\left(\frac{\mathrm{rCMRO_2}(t)}{\mathrm{rCBF}(t)}\right)^{\beta}\right). \tag{6}$$

Assuming that there are no changes in $\mathrm{CMRO_2}$ during hypercapnia (Horvath *et al* 1994), $\mathrm{rCMRO_2}(t) \approx 1$, the hypercapnia calibration parameter H is derived from equation (6):

$$H = \frac{\Delta\mathrm{BOLD}_H(t)/\mathrm{BOLD}_{H0}}{1 - \mathrm{rCBV}_H(t)\mathrm{rCBF}_H(t)^{-\beta}}, \tag{7}$$

where the subscript 'H' denotes the hypercapnia condition. The hypercapnia calibration has been extensively used for quantitative fMRI analyses (Davis *et al* 1998, Hoge *et al* 1999a, Leontiev *et al* 2007, Ances *et al* 2008, Chiarelli *et al* 2007a, 2007b, Wu *et al* 2002). However, there are many sources of bias associated with hypercapnia calibration. Since H is calibrated before the estimation of $\mathrm{CMRO_2}$, possible changes in $\mathrm{CMRO_2}$ cannot be incorporated (Jones *et al* 2002). Furthermore, the changes in $\mathrm{CMRO_2}$ during $\mathrm{CO_2}$ inhalation (Kliefoth *et al* 1979, Jones *et al* 2005, Sicard and Duong 2005) challenge the assumed iso-metabolic condition. This situation may lead to inaccurate estimates of the fractional CBF–$\mathrm{CMRO_2}$ coupling ratio (Chiarelli *et al* 2007b).

Rather than using hypercapnia calibration, the multi-modal approach is therefore proposed in this study to estimate the relative $\mathrm{CMRO_2}$–CBF coupling ratio. Due to simultaneous recording, the coupling ratio derived from the BOLD and NIRS biophysical models should be identical. Hence, using equation (3) and equation (4) gives

$$\mathrm{rCBV}(t)^{-1/\beta}\left(1 - \frac{1}{H}\cdot\frac{\Delta\mathrm{BOLD}(t)}{\mathrm{BOLD_0}}\right)^{1/\beta} = \frac{1+\gamma_r(\Delta\mathrm{HbR}(t)/\mathrm{HbR_0})}{1+\gamma_v(\Delta\mathrm{CBV}(t)/\mathrm{CBV_0})}. \tag{8}$$

At this stage, the unknown parameters are H, β, γ_r, γ_v, CBV_0, and HbR_0. In order to estimate these values, the regression problem is converted as follows:

$$\min_{H,\beta,\gamma_r,\gamma_v,CBV_0,HbR_0} \sum_{i=1}^{N} \left\| \left(\frac{\Delta BOLD(t_i)}{BOLD_0}\right) - H\left(1 - \left(1 + \gamma_0 \frac{\Delta CBV(t_i)}{CBV_0}\right)\left(\frac{1 + \gamma_r\,(\Delta HbR(t_i)/HbR_0)}{1 + \gamma_v\,(\Delta CBV(t_i)/CBV_0)}\right)^{\beta}\right)\right\|_2, \tag{9}$$

where $\{t_i\}_{i=1}^{N}$ denotes the sampling times for the BOLD time series, and $\gamma_0 = 1$ for the CBV from all vasculature. In this equation, $||\cdot||_2$ denotes the l_2 norm. The reason for converting the fitting problem equation (8) to equation (9) is to use NIRS measured oxygen species as covariates to fit the BOLD response.

It turns out that our nonlinear regression problem is severely ill-conditioned due to the redundant parameters. For example, an infinite number of (HbR_0, γ_r) pairs provides the same cost value; thus, HbR_0/γ_r should be estimated as one independent value $\eta_r = HbR_0/\gamma_r$. Furthermore, a previous study (Wu *et al* 2002) suggested that the CBV response in Davis's model comes from the venous compartment, i.e. $\gamma_0 = \gamma_v$ in equation (9). In this case, we can easily see that an infinite number of (CBV_0, γ_v) pairs with the same ratio provide the same cost values. Hence, we should estimate these values as one independent variable $\eta_v = CBV_0/\gamma_v$.

2.4. Estimation of CBF and $CMRO_2$

In the proposed fMRI–NIRS simultaneous recording process, CBF is not measured directly, but is instead estimated using the CBV–CBF relationship. This is done because the changes in CBF and CBV are closely related, as the increase of CBF is triggered by an increase in capillaries and veins, and the increase in the pressure expands the vessels. Grubb *et al* (1974) first described the steady-state relationship between relative CBF and relative CBV on whole brain by changing CBF with inhaled CO_2:

$$rCBV(t) = rCBF(t)^{\alpha}. \tag{10}$$

Here, a value of $\alpha = 0.38$ is typically employed as the power of Grubb *et al* (1974) relationship. However, α has different values depending on the brain region (Wu *et al* 2002, Rapoport *et al* 1979). Furthermore, it is reported that during the transient state the CBF–CBV relationship is not simply governed by the power law.

To explain the transient response in which the CBV values return to their baseline more slowly than CBF after the stimulus is removed (Mandeville *et al* 1998), the balloon model (Buxton *et al* 1998b) and the windkessel model (Mandeville *et al* 1999b) have been proposed. The balloon model assumes that the changes in the blood volume mainly take place in the venous compartment and treats the venous compartment as a distensible balloon. The mass of blood and deoxy-hemoglobin is conserved through the venous balloon. Thus, the rate of volume change is represented as the difference between the inflow $rCBF_{in}(t)$ and the outflow $rCBF_{out}(t)$ with a time constant τ_{MTT}:

$$\frac{d\,(rCBV)}{dt} = \frac{1}{\tau_{MTT}}[rCBF_{in}(t) - rCBF_{out}(t)], \tag{11}$$

where $\tau_{MTT} = CBV_0/CBF_0$ denotes the mean transit time through the volume at rest, $rCBF_{in}(t)$ corresponds to $rCBF(t)$, and $rCBF_{out}(t)$ is described as in an earlier study (Buxton *et al* 1998a):

$$rCBF_{out}(t) = rCBV(t)^{\frac{1}{\alpha}} + \tau_a \frac{d\,(rCBV)}{dt}. \tag{12}$$

Using equations (11) and (12), the relative CBF is given by

$$\mathrm{rCBF}(t) = \mathrm{rCBV}(t)^{1/\alpha} + (\tau_a + \tau_{\mathrm{MTT}}) \frac{\mathrm{d}\,(\mathrm{rCBV})}{\mathrm{d}t}, \tag{13}$$

where α is a constant, τ_{MTT} denotes the mean transit time, and τ_a is a viscoelastic time constant.

Using the estimated relative CBF values, the relative CMRO_2 can be calculated by multiplying the relative CMRO_2–CBF coupling ratio and rCBF:

$$\mathrm{rCMRO}_2(t) = \frac{\widehat{\mathrm{rCMRO}_2}(t)}{\mathrm{rCBF}(t)} \cdot \widehat{\mathrm{rCBF}(t)}, \tag{14}$$

where $\frac{\widehat{\mathrm{rCMRO}(t)}}{\mathrm{rCBF}(t)}$ denotes the estimated relative coupling ratio and $\widehat{\mathrm{rCBF}(t)}$ is the estimated relative CBF, respectively. Although a numerical model is used to estimate the CBF, our framework can be easily incorporated with direct blood flow measurements such as ASL, again without a hypercapnia calibration. In this case, the $\frac{\widehat{\mathrm{rCMRO}_2(t)}}{\mathrm{rCBF}(t)}$ values in equation (14) are measured by NIRS and BOLD simultaneous recording, whereas $\widehat{\mathrm{rCBF}}(t)$ is obtained from ASL measurements.

2.5. *Procedures for estimating $CMRO_2$ and CBF*

The NIRS and BOLD measurements are prone to many noisy factors such as global drifts, vasomotion, blood pressure variation, or long-term physiological changes, etc. Since the amplitude of these bias is often comparable to that of the activated signals, a simple average of NIRS and BOLD response across many blocks often results in bias. This is especially problematic in our case where we need to estimate several calibration parameters by fitting two time traces from different modalities. In order to deal with this issue, we propose a wavelet-based adaptive averaging method for estimating HRF, which is described in the appendix.

After the HRFs are estimated, HbR, HbT, and BOLD time series can be estimated by convolving with the paradigm. The relative CMRO_2–CBF coupling ratio and model parameters including H, β, η_r, and η_v are then estimated from equation (9). This procedure makes the fitting problem more robust than the measurement noise.

The search ranges of model parameters are chosen within the physiological ranges which were estimated from other studies. Specifically, H ranges from 0 to 10% (Kastrup *et al* 2002, Chiarelli *et al* 2007a) and β ranges from 1 to 2 (Davis *et al* 1998, Uludağ *et al* 2004). The venous deoxy-hemoglobin ratio γ_r and venous total-hemoglobin ratio γ_v are both in the range of 0.5–1.5 (Boas *et al* 2003, Mayhew *et al* 2001b). The baseline oxygen saturation SO_2 and total baseline blood volume V_0 ranges from 55 to 80% and 40 to 140 μM, respectively (Boas *et al* 2003, Torricelli *et al* 2001). In order to estimate the accurate parameters, we consider all possible values of unknown parameters by discretizing the parameter search range. All of the search ranges are summarized in table 1.

The optical and MR measurements reflect the changes over the different volume of tissue, which leads to different partial volume effect. Since the partial volume effect affects the accuracy of parameter estimation, it should be corrected. By changing the dynamic properties of the brain layer (scalp, skull, brain) and simulating the CBF in the bottom layer with a semi-infinite medium model, Durduran *et al* (2004) estimated the partial volume effect of NIRS. Since our probe geometry and the experimental protocol are very similar to their simulation condition, we employed the partial volume correction factor p of 6.2 from their work (Durduran *et al* 2004). In particular, we multiply the search range of CBV_0 by the partial

Table 1. Search range from model parameters. The four unknown parameters in our model are H, β, η_r, and η_v. The search space of the combined parameter η_r and η_v is calculated considering feasible parameter ranges of CBV_0, SO_2, γ_r, and γ_v. The partial volume factor p is 6.2 (Durduran *et al* 2004). Due to the space limit, a single representative reference is listed for each row.

Symbol	Description	Search range	References
H	Hypercapnia calibration	[0–10] (%)	Chiarelli *et al* (2007a)
β	Davis's model parameter	[1–2]	Davis *et al* (1998)
η_r	$\eta_r = (1 - SO_2)CBV_0/\gamma_r$	$p \cdot$ [4–126]	
η_v	$\eta_v = CBV_0/\gamma_v$	$p \cdot$ [26–280]	
CBV_0	Total baseline blood volume	[40–140] (μM)	Torricelli *et al* (2001)
SO_2	Baseline oxygen saturation	[55–80] (%)	Boas *et al* (2003)
γ_r	Venous deoxy-hemoglobin ratio	[0.5–1.5]	Boas *et al* (2003)
γ_v	Venous total hemoglobin ratio	[0.5–1.5]	Boas *et al* (2003)

volume factor p (see table 1). Finally, after the estimation of relative $CMRO_2$–CBF coupling and model parameters, the relative CBF and $CMRO_2$ are then calculated using a selected CBV–CBF relationship and equation (14).

3. Method

3.1. Behavior protocol

To evaluate the practicality of the proposed method, a right finger tapping experiment was performed. Subject instruction was visually presented using a beam projector. When the word 'go' appeared, the subjects were to perform a simple finger flexion and extension task repeatedly. When the word 'stop' appeared, the subjects were to stop moving and stare at a fixed point to avoid eye and head movements. As BOLD undershoot was observed for up to 60 s (Bandettini *et al* 1997, Mandeville *et al* 1999a), the finger tapping experiment with a long resting period was performed to investigate the BOLD undershoot. Specifically, a block design sequence consisted of 15 s of task and 72 s of rest in one cycle. The full experimental run consisted of 90 s of rest, followed by four task and rest cycles, followed by an additional 30 s of rest. The total recording time was 468 s. It was expected that the primary motor cortex, somatosensory cortex, and supplementary motor cortex would be mainly activated during finger tapping, based on experimental results from other literature (Witt *et al* 2008). Due to the limit of the penetration depth of the NIRS system, the basal ganglia and cerebellum were excluded from the region of interest (ROI).

3.2. Subject selection

For the finger tapping task, a total of three healthy subjects were examined (mean age = 27 ± 2.6 years). No subject had a history of any neurological disorder. After all of the subjects were given instructions concerning the experimental environment and the operating mode of NIRS and fMRI, signed informed consent forms were obtained. This study was approved by the Institutional Review Board of the Korea Advanced Institute of Science and Technology (KAIST).

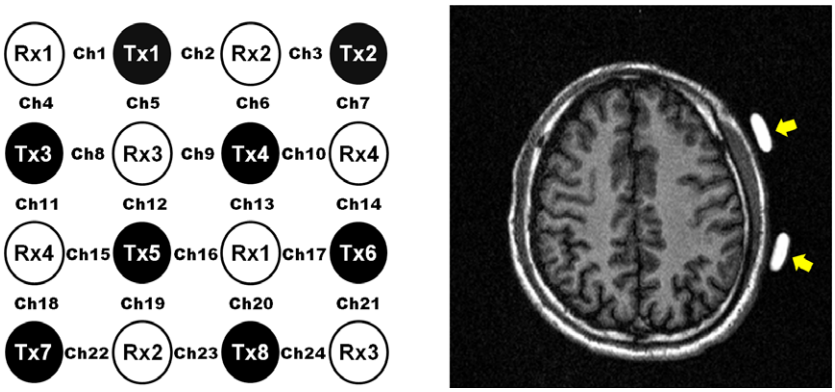

(a) (b)

Figure 1. NIRS channel configuration and optode positions on the subject's head. (a) Schematic diagram of 24 NIRS channels configuration. Tx and Rx denote the illuminator and detector, respectively. Ch denotes the channel. (b) T1-weighted MR image showing the marker capsules highlighted by arrows in an axial section. NIRS channels are localized onto the cerebral cortex of the T1-weighted MR image using Horn's algorithm (Horn *et al* 1987) and the relationship between the MR coordinate and real coordinates is elicited in a 3D digitizer.

3.3. Data acquisition

Experimental data were simultaneously recorded using NIRS and fMRI. Detailed system specifications are described as follows. A continuous wave NIRS instrument (OXYMON MK III, Artinis, the Netherlands) was used to measure the changes in the optical density. The NIRS system emitted 781 nm and 856 nm laser lights at each source fiber. The fiber length was 10 m to connect the optodes in the MR scanner to the NIRS system in the MR control room. The sampling frequency was 10.0 Hz. The NIRS system had 24 channels with eight sources and four detectors, as shown in figure 1(a). The distance between the source and detectors was 3.5 cm. An optode holder cap was attached to the scalp around the left primary motor cortex, somatosensory cortex, and supplementary motor cortex. For spatial registration of the NIRS channels to the Montreal Neurological Institute (MNI) standard space, MR marker capsules were placed on the optode holder cap, as shown in figure 1(b). The marker capsule positions were used to elicit the relationship between the real coordinates and MNI coordinates using Horn's algorithm (Horn *et al* 1987). A 3.0T MRI system (ISOL, Republic of Korea) was used to measure the BOLD response. During the blocked task paradigm, the echo planar imaging (EPI) sequence was used with TR/TE equal to 3000/35 ms, a flip angle of 80°, and 35 slices with a 4 mm slice thickness. In the subsequent anatomical scanning session, T1-weighted structural images were acquired using the same scanner.

3.4. Data analysis

The concentration changes of HbO, HbR, and HbT were calculated from the measured optical density variations using the modified Beer–Lambert law (Cope and Delpy 1988). In order to remove the noise from the NIRS and BOLD time series, Gaussian smoothing with the full width at half-maximum of 2 s was applied. The wavelet–MDL based detrending algorithm (Jang *et al* 2009) was used to eliminate unknown global trends including breathing, subject movement, or instrumental instability.

According to the proposed method, the noise in the measurement was further reduced. HbR, HbT, and BOLD responses during one block of experiment were then estimated. Now,

by solving the regression problem in equation (9), the relative $CMRO_2$–CBF coupling ratio and model parameters were estimated. We selected the channels within the HbT activated region ($p < 0.01$, tube formula correction (Ye *et al* 2009, Sun 1993, Cao and Worsley 1999)) which overlapped with the primary motor cortex, and then estimated model parameters. Finally, the relative CBF and $CMRO_2$ were calculated using equation (10) and equation (14), respectively.

Statistical analyses of estimated CBF and $CMRO_2$ were performed using the software package NIRS-SPM (Ye *et al* 2009, Jang *et al* 2009). Specifically, the general linear model (GLM) (Worsley and Friston 1995), which explains measurements as a linear combination of explanatory variables, provided the Student's *t*-statistics on the interpolated channel positions. Given a specific *p*-value, Sun's tube formula (Sun 1993, Cao and Worsley 1999) was used to calculate an accurate threshold for CBF and $CMRO_2$ activation in an inhomogeneous Gaussian random field. To correct the *p*-value for the BOLD signal, random field correction was applied using a statistical parametric mapping (SPM) package (Wellcome Department of Cognitive Neurology, London, UK) (Friston *et al* 2006). Activated regions were rendered on the brain surface generated from an individual, which is included in the SPM package. Figures 2(a) and (b) show the schematics describing the proposed method of CBF and $CMRO_2$ estimation and corresponding statistical analysis method using NIRS-SPM, respectively. The proposed CBF and $CMRO_2$ quantification method will be included in the NIRS-SPM software package for download (http://bisp.kaist.ac.kr/NIRS-SPM).

4. Results

In order to confirm how well the proposed method estimates the model parameters, we separately generated the relative $CMRO_2$–CBF coupling ratio from BOLD and NIRS models, after solving the fitting problem in equation (9). Figure 3 shows time courses of the estimated $CMRO_2$–CBF coupling ratio on the channels included in the ROI for (a) the first subject, (b) the second subject, and (c) the third subject, respectively. The ROI was selected as the HbT activation area ($p < 0.01$, tube formula correction) which overlapped with the primary motor cortex. Due to variation in channel positions of individuals, the number of channels within the ROI was different between individuals. The solid lines indicate relative $CMRO_2$–CBF coupling ratios from the NIRS biophysical model, whereas the dotted lines indicate those from the BOLD biophysical model. The patterns of the relative $CMRO_2$–CBF coupling ratio from both models were mostly consistent. The coefficient of determination (R^2) from most of the channels is more than 0.9.

Figure 4(a) shows the group average of the estimated HbO, HbR, HbT concentration changes, and fractional BOLD changes. The solid black line denotes the task period. The error bar indicates the standard error of the mean (SEM) across the subjects at each time point. The ROI was selected as the HbT activation area which overlapped with the primary motor cortex. The group average HbO, HbR, and HbT changes during stimulus were $0.65 \pm 0.35\,\mu$M, $-0.06 \pm 0.05\,\mu$M, and $0.56 \pm 0.29\,\mu$M, respectively. The group average of fractional BOLD changes was $0.5 \pm 0.2\%$. Note that post-stimulus undershoot of BOLD and HbT were observed.

Figure 4(b) shows group average time series of the relative $CMRO_2$–CBF coupling ratio. During the post-stimulus, overshoot was estimated. The average hypercapnia parameter H between the subjects was $7.7 \pm 1.7\%$, which is within the range of values estimated in the motor cortex (Kastrup *et al* 2002, Stefanovic *et al* 2004, Chiarelli *et al* 2007a). The average β between the subjects was 1.19 ± 0.23. The β value is known to be 1.5 for the magnetic field strength of 1.5 tesla (Davis *et al* 1998). However, for higher field strengths, it is expected that the BOLD signal mainly comes from the extravascular space, corresponding to a β value

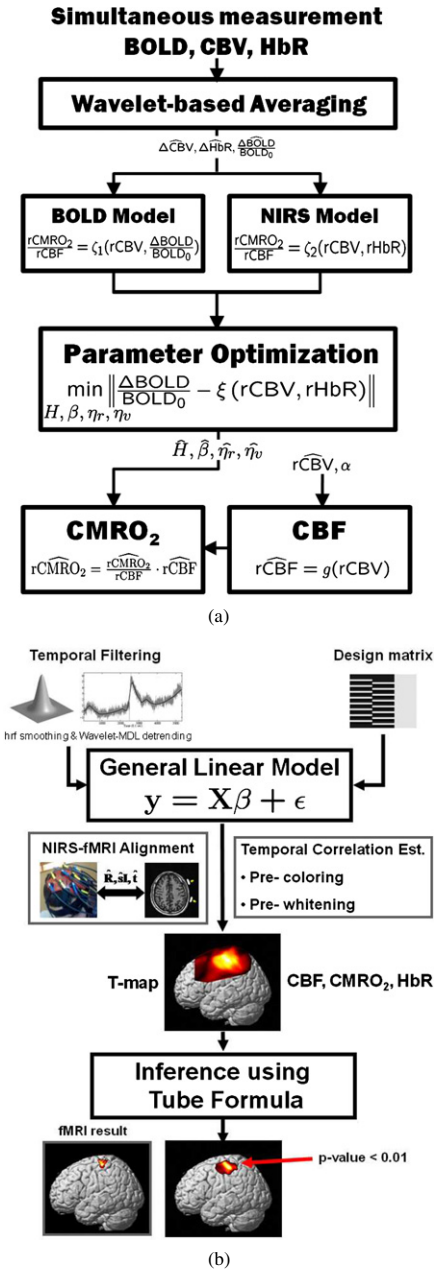

Figure 2. Schematics of cerebral blood flow (CBF)—cerebral metabolic rate of oxygen ($CMRO_2$) estimation method and corresponding statistical analysis method. (a) The proposed method to determine relative $CMRO_2$ ($rCMRO_2$) and relative CBF (rCBF). $\zeta_1(rCBV, \Delta BOLD/BOLD_0)$ and $\zeta_2(rCBV, rHbR)$ denotes the relative $CMRO_2$/CBF ratio from the BOLD biophysical model (Davis *et al* 1998, Hoge *et al* 1999a) and the NIRS biophysical model (Boas *et al* 2003, Mayhew *et al* 2001b), respectively. In the parameter optimization step, $\xi(rCBV, rHbR)$ denotes the biophysical model of fractional BOLD changes. (b) Statistical analysis framework using NIRS-SPM (Ye *et al* 2009, Jang *et al* 2009). Based on the general linear model (Worsley and Friston 1995) and Sun's tube formula (Sun 1993, Cao and Worsley 1999), activated regions from CBF and $CMRO_2$ are extracted.

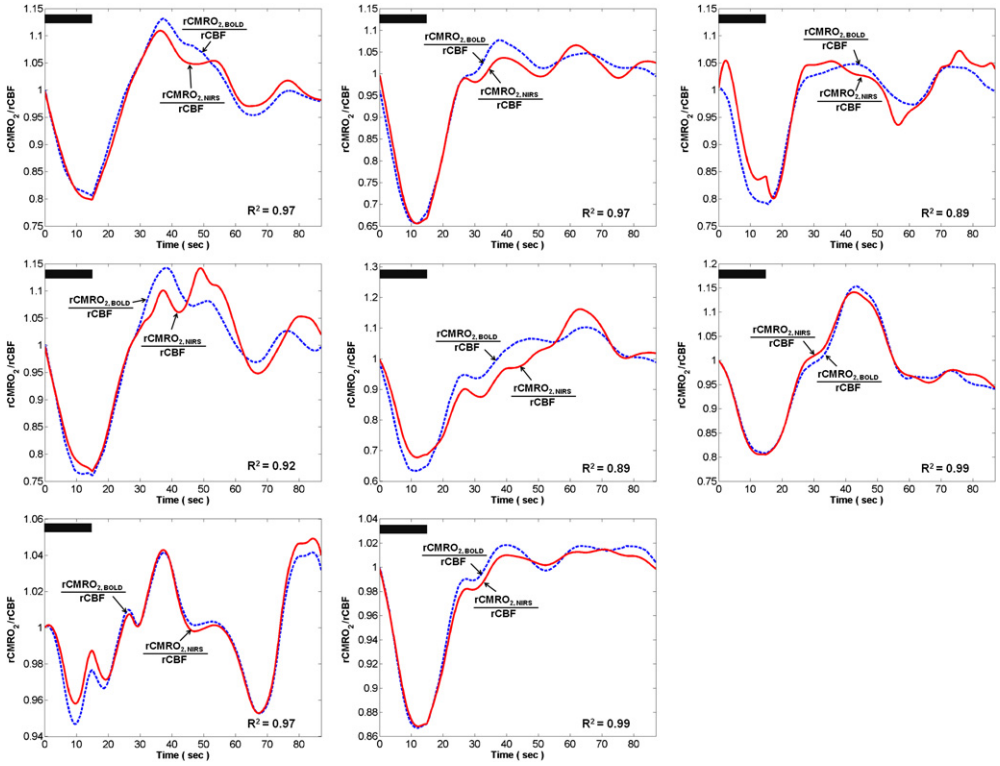

Figure 3. Time courses of the estimated $CMRO_2$–CBF coupling ratio on the channels included in the region of interest (ROI) for (a) the first subject, (b) the second subject and (c) the third subject, respectively. We define the ROI as the total hemoglobin activated region ($p < 0.01$, tube formula correction) which overlapped with the primary motor cortex. The solid lines indicate the relative $CMRO_2$–CBF coupling ratio from the NIRS biophysical model, whereas the dotted lines denote those from the BOLD biophysical model. The coefficient of determination (R^2) from most of the channels is more than 0.9. Due to the variation of channel positions for each individual, the number of channels within the ROI were three for the first and second subjects (figures 3(a) and (b)) and two for the third subject (figure 3(c)).

close to 1 (Buxton 2002). Therefore, in our 3.0T MRI system, the estimated β value is in agreement with the expected value.

The group average time series of the relative CBF and $CMRO_2$ estimates are shown in figure 4(c). The $rCBF_{GM}$ and $rCBF_{BM}$ denote CBF estimated from the Grubb *et al* (1974) relationship ($\alpha = 0.38$) and the balloon model ($\tau = 5$ s) (Buxton *et al* 1998b), respectively. The $rCMRO_{2,GM}$ and $rCMRO_{2,BM}$ denote the relative $CMRO_2$, which are calculated by multiplying the relative flow-metabolism coupling ratio with $rCBF_{GM}$ and $rCBF_{BM}$, respectively. Whereas the balloon model dynamically explains the transient response of CBF and corresponding $CMRO_2$ compared with Grubb's model, the large τ value more than 10 s introduces the pronounced fluctuations. In both models, at the onset of stimulus, CBF rapidly increased, and then persisted over larger fractional changes than $CMRO_2$. Upon the cessation of stimulus, CBF decreased faster than $CMRO_2$. The significant post-stimulus undershoot of CBF was observed. During stimulus, the CBF_{GM} increase was $39.5 \pm 21.4\%$.

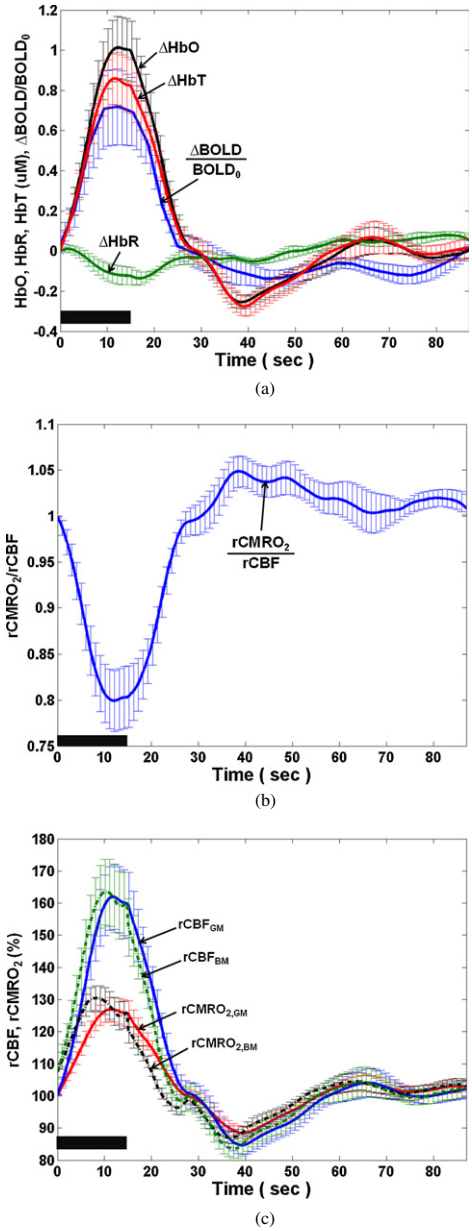

Figure 4. Group average time series of (a) the estimated HbO, HbR, HbT concentration changes, and fractional BOLD changes, (b) relative $CMRO_2$–CBF coupling ratio, and (c) relative CBF (rCBF) and relative $CMRO_2$ ($rCMRO_2$) estimates from the finger tapping experiment. The $rCBF_{GM}$ and $rCBF_{BM}$ denote rCBF estimated from the Grubb *et al* (1974) relationship ($\alpha = 0.38$) and the balloon model ($\tau = 5$ s) (Buxton *et al* 1998b), respectively. The $rCMRO_{2,GM}$ and $rCMRO_{2,BM}$ denotes the $rCMRO_2$ which was calculated as multiplying the relative flow-metabolism coupling ratio and $rCBF_{GM}$ and $rCBF_{BM}$, respectively. The solid black line denotes the task period. The error bar indicates the standard error of the mean (SEM) across the subjects at each time point. The region of interest is the total hemoglobin activation region ($p < 0.01$, tube formula correction) which overlapped with the primary motor cortex. During stimulus, the change in $rCBF_{GM}$ was $39.5 \pm 21.4\%$. The change in $rCMRO_{2,GM}$ was $18.4 \pm 8.7\%$.

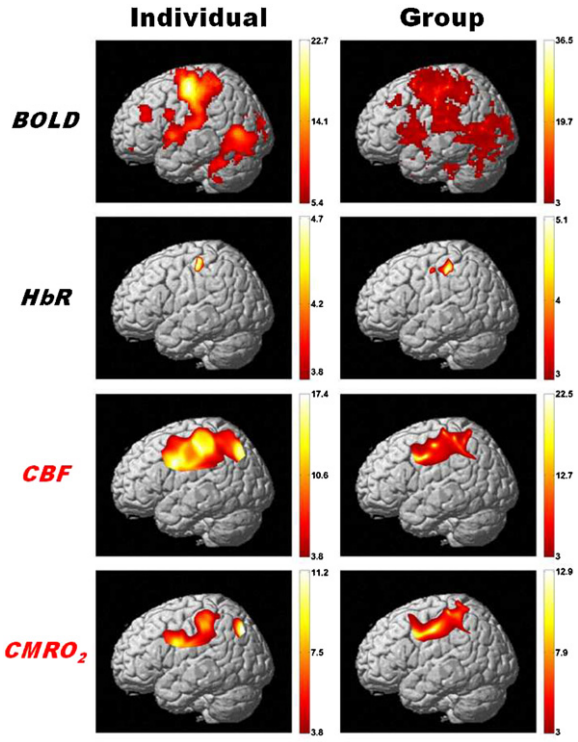

Figure 5. Activation areas from BOLD, HbR, CBF, and $CMRO_2$ during the finger tapping task. The first column shows the individual activation patterns ($p < 0.01$, BOLD : random field correction, NIRS : tube formula correction). The second column shows the group activation patterns ($p < 0.05$, uncorrected) during the finger tapping task. The activated region of CBF corresponds well with that of $CMRO_2$ and the target region of the finger tapping task. $CMRO_2$ activation was more tightly localized on the primary motor cortex, compared with CBF activation.

The change in $CMRO_{2,GM}$ was $18.4 \pm 8.7\%$. The fractional CBF–$CMRO_2$ coupling ratio $n(t)$ is then calculated as follows:

$$n(t) = \frac{\mathrm{rCBF}(t) - 1}{\mathrm{rCMRO_2}(t) - 1}. \tag{15}$$

Note that this is different from the *relative* $CMRO_2$–CBF coupling ratio, $\mathrm{rCMRO_2}(t)/\mathrm{rCBF}(t)$, which results from the proposed fitting procedure. The group average of fractional $CMRO_2$–CBF coupling ratio, n, was 2.38 ± 0.65. This coupling ratio is within the range of 2–4 reported from many other studies (Boas *et al* 2003, Hoge *et al* 1999a, 2005, Durduran *et al* 2004, Sheth *et al* 2004, Kastrup *et al* 2002, Kim *et al* 1999, Davis *et al* 1998).

Individual activation patterns from the simultaneously measured BOLD signal ($p < 0.01$, random-field correction), HbR, CBF, and $CMRO_2$ ($p < 0.01$, tube formula correction) are shown in the first column of figure 5. Group activation patterns ($p < 0.05$, uncorrected) are shown in the second column of figure 5. BOLD activations were observed in the premotor area, primary motor cortex and somatosensory cortex, which are the main target region of finger tapping task (Witt *et al* 2008). HbR activation was tightly localized on the primary motor cortex. Activated spots of CBF corresponded well with that of $CMRO_2$ and ROI of

finger tapping task. Note that $CMRO_2$ activation was more localized to the primary motor cortex, compared with CBF activation.

5. Discussion

5.1. Interpretation of the fractional CBF–$CMRO_2$ coupling ratio

The determination of the fractional coupling ratio between CBF and $CMRO_2$, n, is important for the quantitative interpretation of the activated BOLD signal. A different n value for the same changes in $CMRO_2$ induces a large difference in the BOLD changes. The fractional coupling ratio between CBF and $CMRO_2$ was originally investigated by Fox and Raichle (1986). Numerous studies have reported the values of n in the range of 2–4 (Boas *et al* 2003, Hoge *et al* 1999a, 2005, Durduran *et al* 2004, Sheth *et al* 2004, Kastrup *et al* 2002, Kim *et al* 1999, Davis *et al* 1998). The different fractional changes in CBF and $CMRO_2$ can be explained by the oxygen limitation model (Buxton and Frank 1997, Gjedde *et al* 1991), which asserts that a large increase of CBF accompanied by a small decrease of the oxygen-extraction factor can produce a fractional increase of $CMRO_2$. Physiologically, the decrease of the oxygen extraction factor can be explained based on two assumptions: (1) the increase in CBF is accomplished by increased capillary blood velocity rather than by capillary recruitment (Bereczki *et al* 1993); (2) oxygen delivery to tissue is limited at rest (Gjedde *et al* 1991) so that only a fraction of the oxygen delivered to the capillary bed is extracted from the blood and becomes available for metabolism. More specifically, oxygen diffusion from capillary plasma to the mitochondria is managed by the gradient of partial pressure of oxygen (pO_2) between the capillary and the tissue. To increase $CMRO_2$, the average capillary pO_2 should increase and consequently oxygen extraction should decrease, as the fractional saturation of oxy-hemoglobin, which is a function of the plasma partial pressure of oxygen, has a sigmoidal shape (Buxton and Frank 1997, Buxton 2002). At a steady-state condition, relative $CMRO_2$ is proportional to the ratio of relative CBF and relative oxygen-extraction fraction $\mathrm{rOEF}(t)$ (Buxton 2002): $\mathrm{rCMRO_2}(t) = \mathrm{rOEF}(t)/\mathrm{rCBF}(t)$. Due to the decrease in the oxygen-extraction fraction induced by the CBF increase, CBF should increase more compared to $CMRO_2$.

5.2. The relationship between CBF and CBV

The changes in CBF are closely related to the changes in CBV. Specifically, CBF increases are generated by drops in the arteriole resistance, that lead to increases in the pressure of capillaries and veins. The increase in the pressure expands the vessels (Grubb *et al* 1974), describing the steady-state relationship between CBF and CBV as the empirically derived power law shown in equation (10). However, since Grubb's law is based on the steady-state measurements of whole brain, it has limitations for explaining the transient relationship between CBF and CBV in a specific brain region. Previous studies found that the power factor α changes with different brain regions (Wu *et al* 2002, Rapoport *et al* 1979) or different vascular compartments (Zheng and Mayhew 2009). Furthermore, the α value is typically lower under stimulation than during hypercapnia and ranges from 0.18–0.36 depending on the simulation duration (Mandeville *et al* 1999b, Jones *et al* 2001, 2002). During transient phases of vessel dilation and contraction, dynamic relationships between CBF and CBV are not simply expressed as the power law, which suggests additional terms for explaining the transient behaviors.

The difference between the transient-state characteristics of CBF and CBV comes from the visco-elastic properties of vessels. Viscoelasticity of venous vessels leads the vessel

volume to increase rapidly upon the onset of stimulus and slowly decrease upon the cessation of stimulus. The works in Buxton *et al* (1998a, 1998b) considered these viscoelastic effects in the CBF as the rate of CBV changes. According to equation (13), the balloon initially resists the changes in CBV and finally arrives at a steady state. The time constant τ controls the time required to adjust to a transient state. Similarly, Mandeville *et al* (1999b), Zheng and Mayhew (2009), and Huppert *et al* (2009) described capillary and venous compliance as windkessel theory passively responding to arterial pressure changes.

Figure 4(c) shows the group average CBF response estimated using the Grubb *et al* (1974) model (GM) and the balloon model (BM) (Buxton *et al* 1998b). The balloon model dynamically explains the transient response of CBF and corresponding $CMRO_2$, compared with Grubb's model. As the value of α decreases, the changes in CBF increase. In the balloon model, as the τ value increases, CBF increases more rapidly upon the onset of stimulus and more promptly decreases after cessation of stimulus.

Note that the limitation of our current estimation of $CMRO_2$ is dependent upon the accuracy of the CBF model. Hence, for the accurate estimation of $rCMRO_2$ a direct flow measurement will be useful. However, even with the separate flow measurement, our $rCMRO_2$/rCBF coupling ratio is still valid since these quantities are obtained from fMRI–NIRS simultaneous recording.

5.3. Post-stimulus undershoot of CBF and $CMRO_2$

In our experiments, the undershoot of the CBF response during post-stimulus was consistently observed using Grubb's model or the balloon model, etc. (Grubb *et al* 1974, Jones *et al* 2002, Buxton *et al* 1998a, 1998b, 2004). Therefore, it is likely that the post-stimulus undershoot of CBF, as shown in figure 4(c), did not stem from an inaccurate choice of parameters of the Grubb model or the balloon model, but rather from the inherent characteristics of the data. A number of studies have observed CBF undershoot (Hoge *et al* 1999a, 1999b, Uludağ *et al* 2004, Huppert *et al* 2009, 2006, Chen and Pike 2009, Obata *et al* 2004, Sheth *et al* 2004, Durduran *et al* 2004, Davis *et al* 1998). However, in many other studies, CBF undershoot was not observed (Lu *et al* 2004, Shen *et al* 2008, Kruger *et al* 1998, Hoge *et al* 2005, Kida *et al* 2007). Although the reasons for this difference remain controversial, the type of stimulus or the experimental paradigm (Hoge *et al* 1999b) and an autoregulatory CBF feedback mechanism of neuronal origin (Friston *et al* 2000, Uludağ *et al* 2004) are the possible sources of these inconsistency.

In our setup, the CBF response is not directly measured by the NIRS system. Hence, the CBF undershoot is numerically determined by the CBV undershoot. Many optical studies estimate the CBF undershoot corresponding to the CBV undershoot (Sheth *et al* 2004, Huppert *et al* 2009, 2006, Durduran *et al* 2004). Assuming that the hematocrit is constant, the changes in CBV are related to the changes in HbT. However, considering the evidence of the hematocrit changes in the vascular compartment (Mchedlishvili 1986), an elaborate relationship between CBV and HbT would provide more reliable observations regarding the CBV response in the NIRS system.

Figure 4(c) describes the group average $CMRO_2$ responses corresponding to CBF estimates from Grubb's model. Post-stimulus undershoot of $CMRO_2$ was also observed. In our method, the changes in $CMRO_2$ are determined by multiplying the relative $CMRO_2$–CBF coupling ratio by the estimated CBF changes. We observed that the dynamic range of the relative coupling ratios were not as large as that of CBF. Since the $CMRO_2$ is calculated using equation (14), the CBF undershoot therefore results in $CMRO_2$ undershoot. Although real flow measurements using ASL may be necessary to confirm whether the $CMRO_2$ undershoot really

comes from the neurovascular coupling mechanism, it is still interesting to note that several previous studies exhibit the post-stimulus $CMRO_2$ undershoot from optical measurements (Sheth *et al* 2004, Durduran *et al* 2004, Jones *et al* 2001) and MR measurements (Davis *et al* 1998, Mandeville *et al* 1999a).

5.4. Post-stimulus undershoot of the BOLD response

In this study, the undershoot of the BOLD response during post-stimulus was observed, as shown in figure 4(a). BOLD undershoot is strongly influenced by the transient increase of the local deoxy-hemoglobin level. Currently, three theories to explain the post-stimulus undershoot of the BOLD response have been proposed. First, assuming that the CBF response rapidly returns to its baseline, the delayed recovery of CBV may accumulate the HbR content, which would then lead to BOLD undershoot (Buxton *et al* 1998b, Mandeville *et al* 1999b, Chen and Pike 2009). This observation has been embodied in biomechanical models such as the balloon model (Buxton *et al* 1998b) and the windkessel model (Mandeville *et al* 1999b). Second, the prolonged elevation of $CMRO_2$ has been postulated as the sole contributor of BOLD undershoot, in the presence of rapid CBF and CBV returns (Frahm *et al* 2008, 1996, Lu *et al* 2004, Kruger *et al* 1999). According to this theory, in order to replenish the ionic gradient that was decreased by action potential generation, $CMRO_2$ is elevated upon the cessation of stimulus (Lu *et al* 2004). However, as recent research clearly shows that the magnitude and duration of BOLD undershoot do not depend on the intensity or duration of the stimulus (Chen and Pike 2009), it is uncertain that the elevated $CMRO_2$ is the sole contributor to BOLD undershoot. Third, CBF undershoot as well as the slow recovery of venous CBV has been postulated to contribute to the post-stimulus undershoot of the BOLD response (Chen and Pike 2009). Using a set of measures consisting of the amplitude, full width at half-maximum (FHWM), and time to fall of the post-stimulus undershoot, these studies have shown that the amplitude and duration of CBF undershoot were significantly correlated with those of BOLD undershoot during post-stimulus.

In the experimental results of this study (figure 4), the undershoot of CBV and the overshoot of the relative $CMRO_2$–CBF coupling ratio ($rCMRO_2(t)/rCBF(t)$) were consistently observed. According to Davis' model, in equation (6), the relative CBV and the $CMRO_2$–CBF coupling ratio are the two main factors that determine the BOLD undershoot. Although the CBV undershoot has a negative effect on the BOLD undershoot, larger overshoot of the relative $CMRO_2$–CBF coupling ratio results in the BOLD undershoot. In our data, the dynamic range of the relative coupling ratio was larger than that of CBV, suggesting that the relative coupling ratio was the main contributor of BOLD post-stimulus undershoot. This implies that the transient decoupling between the metabolism and the blood flow is the main source of BOLD undershoot.

6. Conclusion

A CBF and $CMRO_2$ estimation method was developed from simultaneous measurements of NIRS and BOLD. The proposed multimodal approach readily estimated CBF and $CMRO_2$ without any separate calibration under hypercapnia, hyperoxia, and breath-holding conditions. The relative $CMRO_2$–CBF coupling ratio was calculated by fitting biophysical models from NIRS and BOLD measurements. Then, $CMRO_2$ was estimated by multiplying the coupling ratio with CBF. Optimizing many unknown parameters within the physiological range greatly enhanced the accuracy of the proposed method. Experimental results from a finger tapping task showed that the estimated CBF and $CMRO_2$ time series were in good agreement with

physiological findings of other studies. The coupling ratio between CBF and $CMRO_2$ was also within the range of other studies. The CBF calculations from various models conducted in this study suggest that CBF exhibits post-stimulus undershoot whose magnitude variation is greater than that of $CMRO_2$, explaining the origin of the BOLD post-stimulus undershoot. Furthermore, the activated regions from CBF and $CMRO_2$ were localized on the primary motor cortex, which was the main target region of the finger tapping task.

Acknowledgments

The authors would like to thank David Boas at Harvard for valuable comments that significantly helped to enhance the contents of this paper. This research was supported by the Korea Science and Engineering Foundation (KOSEF) grant funded by the Korean government (MEST) (no 2009-0081089).

Appendix

We assume that the measurement at the ith channel is given by

$$y^{(i)}(t) = (\theta^{(i)} * s)(t) + n^{(i)}(t), \tag{A.1}$$

where $\theta^{(i)}$ denotes the hemodynamic response function (HRF), s is the input paradigm response, and $n^{(i)}$ is the noise contributor, respectively. In the proposed wavelet averaging, the HRF is represented as

$$\theta^{(i)}(t) = a\theta_J[0]\Phi(2^{-J}t) + \sum_{j=J_0}^{J}\sum_{k=0}^{2^{-j}M-1} \mathrm{d}\theta_j[k]\psi(2^{-j}t - k), \tag{A.2}$$

where $\psi(t)$ is the wavelet and $\Phi(t)$ is the scaling function associated with a multiresolution analysis (Mallat 1999), J_0 denotes the finest scale that determines the smoothness of the trend, and the wavelet coefficients composed of approximation coefficients $\{a\theta_j[k]\}_{j,k}$ and detail coefficients $\{\mathrm{d}\theta_j[k]\}_{j,k}$ are defined by the following recursions (Mallat 1999):

$$\begin{aligned}
a\theta_0[k] &= \theta[k], && k = 0, \ldots, M-1 \\
a\theta_{j+1}[k] &= \sum_n h[n-2k]a\theta_j[n], && k = 0, \ldots, 2^{-j-1}M - 1 \\
\mathrm{d}\theta_{j+1}[k] &= \sum_n g[n-2k]a\theta_j[n], && k = 0, \ldots, 2^{-j-1}M - 1,
\end{aligned}$$

where $j = 0, \ldots, J-1$, J is the maximum level of wavelet decomposition, $M \approx 2^J$, h is the low-pass filter, and g is the high-pass filter, respectively.

In equation (A.2), the paradigm related input s is known, and our goal is to estimate the hemodynamic response θ. In order to estimate the correct model order, our cost function is derived based on MDL principle for NIRS (Rissanen 1978, Jang *et al* 2009) and SIC principle for BOLD (Schwarz *et al* 1978, Meyer *et al* 2003):

$$c(n_0) = \frac{N}{2}\log\hat{\sigma}^2(n_0) + L(n_0), \tag{A.3}$$

where

$$L(n_0) = \begin{cases} \frac{3}{2}n_0 \log M: & \text{NIRS} \\ \frac{1}{2}n_0 \log M: & \text{BOLD,} \end{cases}$$

and

$$\hat{\sigma}^2(n_0) = \frac{1}{N}\left\| y^{(i)} - \left(a\theta_J[0](\Phi(2^{-J}t) * s) + \sum_{j=J_0}^{J} \sum_{k=0}^{2^{-j}M-1} \mathrm{d}\theta_j[k](\psi(2^{-j}t - k) * s) \right) \right\|_2^2.$$

Here, n_0 denotes the number of non-zero coefficients in wavelet decomposition. The reason we use the different type of $L(n_0)$ for NIRS and BOLD is their different asymptotic behaviors depending on the length of time series (see details in Jang *et al* (2009)). In order to find the optimal parameter n_0 for equation (A.3), we perform the LASSO regression (Tibshirani *et al* 1996). More specifically, LASSO adds basis one by one along the homotopy path. In our approach, at each homotopy path, the cost in equation (A.3) is calculated, and the n_0 value that minimizes equation (A.3) is chosen as the optimal number of non-zero wavelet coefficients.

References

Ances B, Buerk D, Greenberg J and Detre J 2001 Temporal dynamics of the partial pressure of brain tissue oxygen during functional forepaw stimulation in rats *Neurosci. Lett.* **306** 106–10

Ances B, Leontiev O, Perthen J, Liang C, Lansing A and Buxton R 2008 Regional differences in the coupling of cerebral blood flow and oxygen metabolism changes in response to activation: implications for BOLD–fMRI *NeuroImage* **39** 1510–21

Bandettini P, Kwong K, Davis T, Tootell R, Wong E, Fox P, Belliveau J, Weisskoff R and Rosen B 1997 Characterization of cerebral blood oxygenation and flow changes during prolonged brain activation *Hum. Brain Mapp.* **5** 93–109

Bereczki D, Wei L, Otsuka T, Acuff V, Pettigrew K, Patlak C and Fenstermacher J 1993 Hypoxia increases velocity of blood flow through parenchymal microvascular systems in rat brain *J. Cereb. Blood Flow Metab.* **13** 475–86

Boas D, Strangman G, Culver J, Hoge R, Jasdzewski G, Poldrack R, Rosen B and Mandeville J 2003 Can the cerebral metabolic rate of oxygen be estimated with near-infrared spectroscopy? *Phys. Med. Biol.* **48** 2405–18

Boxerman J, Bandettini P, Kwong K, Baker J, Davis T, Rosen B and Weisskoff R 1995 The intravascular contribution to fMRI signal change: Monte Carlo modeling and diffusion-weighted studies *in vivo Magn. Reson. Med.* **34** 4–10

Buxton R 2002 *Introduction to Functional Magnetic Resonance Imaging: Principles and Techniques* (New York: Cambridge University Press)

Buxton R and Frank L 1997 A model for the coupling between cerebral blood flow and oxygen metabolism during neural stimulation *J. Cereb. Blood Flow Metab.* **17** 64–72

Buxton R, Miller K, Frank L and Wong E 1998a BOLD signal dynamics: the balloon model with viscoelastic effects *Sixth Meeting, Int. Society for Magnetic Resonance in Medicine (Sydney, Australia)* p 1401

Buxton R, Uludağ K, Dubowitz D and Liu T 2004 Modeling the hemodynamic response to brain activation *NeuroImage* **23** 220–33

Buxton R, Wong E and Frank L 1998b Dynamics of blood flow and oxygenation changes during brain activation: the balloon model *Magn. Reson. Med.* **39** 855–64

Cao J and Worsley K 1999 The detection of local shape changes via the geometry of Hotellings T^2-fields *Ann. Stat.* **27** 925–42

Chen J and Pike G 2009 Origins of the BOLD post-stimulus undershoot *NeuroImage* **46** 559–68

Chiarelli P, Bulte D, Gallichan D, Piechnik S, Wise R and Jezzard P 2007a Flow-metabolism coupling in human visual, motor, and supplementary motor areas assessed by magnetic resonance imaging *Magn. Reson. Med.* **57** 538–47

Chiarelli P, Bulte D, Piechnik S and Jezzard P 2007b Sources of systematic bias in hypercapnia-calibrated functional MRI estimation of oxygen metabolism *NeuroImage* **34** 35–43

Chiarelli P, Bulte D, Wise R, Gallichan D and Jezzard P 2007c A calibration method for quantitative BOLD–fMRI based on hyperoxia *NeuroImage* **37** 808–20

Cope M and Delpy D 1988 System for long-term measurement of cerebral blood and tissue oxygenation on newborn infants by near infra-red transillumination *Med. Biol. Eng. Comput.* **26** 289–94

Davis T, Kwong K, Weisskoff R and Rosen B 1998 Calibrated functional MRI: mapping the dynamics of oxidative metabolism *Proc. Natl Acad. Sci. USA* **95** 1834–9

Durduran T, Yu G, Burnett M, Detre J, Greenberg J, Wang J, Zhou C and Yodh A 2004 Diffuse optical measurement of blood flow, blood oxygenation, and metabolism in a human brain during sensorimotor cortex activation *Opt. Lett.* **29** 1766–8

Fox P and Raichle M 1986 Focal physiological uncoupling of cerebral blood flow and oxidative metabolism during somatosensory stimulation in human subjects *Proc. Natl Acad. Sci. USA* **83** 1140–4

Frahm J, Baudewig J, Kallenberg K, Kastrup A, Merboldt K and Dechent P 2008 The post-stimulation undershoot in BOLD–fMRI of human brain is not caused by elevated cerebral blood volume *NeuroImage* **40** 473–81

Frahm J, Kruger G, Merboldt K and Kleinschmidt A 1996 Dynamic uncoupling and recoupling of perfusion and oxidative metabolism during focal brain activation in man *Magn. Reson. Med.* **35** 143–8

Friston K J, Ashburner J, Kiebel S, Nichols T and Penny W (ed) 2006 *Statistical Parametric Mapping: The Analysis of Functional Brain Images* (San Diego, CA: Academic)

Friston K, Mechelli A, Turner R and Price C 2000 Nonlinear responses in fMRI: the balloon model, Volterra kernels, and other hemodynamics *NeuroImage* **12** 466–77

Gjedde A, Ohta S, Kuwabara H and Meyer E 1991 Is oxygen diffusion limiting for blood-brain transfer of oxygen? *Brain Work and Mental Activity: Alfred Benzon Symp. (Munksgaard Copenhagen)* vol 31 ed N Lassen, D Ingvar, M Raichle and L Friberg pp 177–84

Gordon G, Choi H, Rungta R, Ellis-Davies G and MacVicar B 2008 Brain metabolism dictates the polarity of astrocyte control over arterioles *Nature* **456** 745–50

Grubb R, Raichle M, Eichling J and Ter-pogossian M 1974 The effects of changes in PaCO2 cerebral blood volume, blood flow, and vascular mean transit time *Stroke* **5** 630–9

Hein T, Xu W and Kuo L 2006 Dilation of retinal arterioles in response to lactate: role of nitric oxide, guanylyl cyclase, and ATP-sensitive potassium channels *Invest. Ophthalmol. Vis. Sci.* **47** 693–9

Hoge R, Atkinson J, Gill B, Crelier G, Marrett S and Pike G 1999a Investigation of BOLD signal dependence on cerebral blood flow and oxygen consumption: the deoxyhemoglobin dilution model *Magn. Reson. Med.* **42** 849–63

Hoge R, Atkinson J, Gill B, Crelier G, Marrett S and Pike G 1999b Stimulus-dependent BOLD and perfusion dynamics in human V1 *NeuroImage* **9** 573–85

Hoge R, Franceschini M, Covolan R, Huppert T, Mandeville J and Boas D 2005 Simultaneous recording of task-induced changes in blood oxygenation, volume, and flow using diffuse optical imaging and arterial spin-labeling MRI *NeuroImage* **25** 701–7

Horn B *et al* 1987 Closed-form solution of absolute orientation using unit quaternions *J. Opt. Soc. Am.* A **4** 629–42

Horvath I, Sandor N, Ruttner Z and McLaughlin A 1994 Role of nitric oxide in regulating cerebrocortical oxygen consumption and blood flow during hypercapnia *J. Cereb. Blood Flow Metab.* **14** 503–9

Hu Y and Wilson G 2002 A temporary local energy pool coupled to neuronal activity: fluctuations of extracellular lactate levels in rat brain monitored with rapid-response enzyme-based sensor. *J. Neurochem.* **69** 1484–90

Huppert T, Allen M, Diamond S and Boas D 2009 Estimating cerebral oxygen metabolism from fMRI with a dynamic multi-compartment windkessel model *Hum. Brain Mapp.* **30** 1548–67

Huppert T, Hoge R, Diamond S, Franceschini M and Boas D 2006 A temporal comparison of BOLD, ASL, and NIRS hemodynamic responses to motor stimuli in adult humans *NeuroImage* **29** 368–82

Jang K, Tak S, Jung J, Jang J, Jeong Y and Ye J 2009 Wavelet minimum description length detrending for near-infrared spectroscopy *J. Biomed. Opt.* **14** 034004

Jones M, Berwick J, Hewson-Stoate N, Gias C and Mayhew J 2005 The effect of hypercapnia on the neural and hemodynamic responses to somatosensory stimulation *NeuroImage* **27** 609–23

Jones M, Berwick J, Johnston D and Mayhew J 2001 Concurrent optical imaging spectroscopy and laser-doppler flowmetry: the relationship between blood flow, oxygenation, and volume in rodent barrel cortex *NeuroImage* **13** 1002–15

Jones M, Berwick J and Mayhew J 2002 Changes in blood flow, oxygenation, and volume following extended stimulation of rodent barrel cortex *NeuroImage* **15** 474–87

Kasischke K, Vishwasrao H, Fisher P, Zipfel W and Webb W 2004 Neural activity triggers neuronal oxidative metabolism followed by astrocytic glycolysis *Science* **305** 99–103

Kastrup A, Krüger G, Glover G and Moseley M 1999 Assessment of cerebral oxidative metabolism with breath holding and fMRI *Magn. Reson. Med.* **42** 608–11

Kastrup A, Kruger G, Neumann-Haefelin T, Glover G and Moseley M 2002 Changes of cerebral blood flow, oxygenation, and oxidative metabolism during graded motor activation *NeuroImage* **15** 74–82

Kida I, Rothman D and Hyder F 2007 Dynamics of changes in blood flow, volume, and oxygenation: implications for dynamic functional magnetic resonance imaging calibration *J. Cereb. Blood Flow Metab.* **27** 690–6

Kim S, Rostrup E, Larsson H, Ogawa S and Paulson O 1999 Determination of relative $CMRO_2$ from CBF and BOLD changes: significant increase of oxygen consumption rate during visual stimulation *Magn. Reson. Med.* **41** 1152–61

Kliefoth A, Grurb R and Raichle M 1979 Depression of cerebral oxygen utilization by hypercapnia in the rhesus monkey *J. Neurochem.* **32** 661–3

Kruger G, Kastrup A, Takahashi A and Glover G 1999 Simultaneous monitoring of dynamic changes in cerebral blood flow and oxygenation during sustained activation of the human visual cortex. *NeuroReport* **10** 2939–43

Kruger G, Kleinschmidt A and Frahm J 1998 Stimulus dependence of oxygenation-sensitive MRI responses to sustained visual activation. *NMR Biomed.* **11** 75–9

Leontiev O, Dubowitz D and Buxton R 2007 CBF/$CMRO_2$ coupling measured with calibrated BOLD fMRI: sources of bias *NeuroImage* **36** 1110–22

Lu H, Golay X, Pekar J and van Zijl P 2004 Sustained poststimulus elevation in cerebral oxygen utilization after vascular recovery *J. Cereb. Blood Flow Metab.* **24** 764–70

Mallat S G 1999 *A Wavelet Tour of Signal Processing* (San Diego, CA: Academic)

Malonek D, Dirnagl U, Lindauer U, Yamada K, Kanno I and Grinvald A 1997 Vascular imprints of neuronal activity: relationships between the dynamics of cortical blood flow oxygenation and volume changes following sensory stimulation *Proc. Natl Acad. Sci. USA* **94** 14826–31

Mandeville J, Marota J, Ayata C, Moskowitz M, Weisskoff R and Rosen B 1999a MRI measurement of the temporal evolution of relative $CMRO_2$ during rat forepaw stimulation *Magn. Reson. Med.* **42** 944–51

Mandeville J, Marota J, Ayata C, Zaharchuk G, Moskowitz M, Rosen B and Weisskoff R 1999b Evidence of a cerebrovascular postarteriole windkessel with delayed compliance *J. Cereb. Blood Flow Metab.* **19** 679–89

Mandeville J, Marota J, Kosofsky B, Keltner J, Weissleder R, Rosen B and Weisskoff R 1998 Dynamic functional imaging of relative cerebral blood volume during rat forepaw stimulation *Magn. Reson. Med.* **39** 615–24

Mayhew J, Johnston D, Berwick J, Jones M, Coffey P and Zheng Y 2001a Erratum and addendum: spectroscopic analysis of neural activity in brain. Increased oxygen consumption following activation of barrel cortex *NeuroImage* **13** 540–3

Mayhew J, Johnston D, Martindale J, Jones M, Berwick J and Zheng Y 2001b Increased oxygen consumption following activation of brain: theoretical footnotes using spectroscopic data from barrel cortex *NeuroImage* **13** 975–87

Mchedlishvili G 1986 *Arterial Behavior and Blood Circulation in the Brain* (New York: Plenum)

Meyer F 2003 Wavelet-based estimation of a semiparametric generalized linear model of fMRI time-series *IEEE Trans. Med. Imaging* **22** 315–22

Mukamel R, Gelbard H, Arieli A, Hasson U, Fried I and Malach R 2005 Coupling between neuronal firing, field potentials, and fMRI in human auditory cortex *Science* **309** 951–4

Obata T, Liu T, Miller K, Luh W, Wong E, Frank L and Buxton R 2004 Discrepancies between BOLD and flow dynamics in primary and supplementary motor areas: application of the balloon model to the interpretation of BOLD transients *NeuroImage* **21** 144–53

Rapoport S, Ohno K and Pettigrew K 1979 Drug entry into the brain. *Brain Res.* **172** 354–9

Rissanen J 1978 Modeling by shortest data description *Automatica* **14** 465–71

Schummers J, Yu H and Sur M 2008 Tuned responses of astrocytes and their influence on hemodynamic signals in the visual cortex *Science* **320** 1638–43

Schwarz 1978 Estimating the dimension of a model *Ann. Stat.* **6** 461–4

Shen Q, Ren H and Duong T 2008 CBF, BOLD, CBV, and $CMRO_2$ fMRI signal temporal dynamics at 500-msec resolution *J. Magn. Reson. Imaging* **27** 599–606

Sheth S, Nemoto M, Guiou M, Walker M, Pouratian N and Toga A 2004 Linear and nonlinear relationships between neuronal activity, oxygen metabolism, and hemodynamic responses *Neuron* **42** 347–55

Sicard K and Duong T 2005 Effects of hypoxia, hyperoxia, and hypercapnia on baseline and stimulus-evoked BOLD, CBF, and $CMRO_2$ in spontaneously breathing animals *NeuroImage* **25** 850–8

Smith A, Blumenfeld H, Behar K, Rothman D, Shulman R and Hyder F 2002 Cerebral energetics and spiking frequency: the neurophysiological basis of fMRI *Proc. Natl Acad. Sci. USA* **99** 10765–70

Stefanovic B, Warnking J and Pike G 2004 Hemodynamic and metabolic responses to neuronal inhibition *NeuroImage* **22** 771–8

Sun J 1993 Tail probabilities of the maxima of Gaussian random fields *Ann. Probab.* **21** 34–71

Tibshirani R 1996 Regression shrinkage and selection via the lasso *J. R. Statist. Soc. B* **58** 267–88

Torricelli A, Pifferi A, Taroni P, Giambattistelli E and Cubeddu R 2001 *In vivo* optical characterization of human tissues from 610 to 1010 nm by time-resolved reflectance spectroscopy *Phys. Med. Biol.* **46** 2227–38

Uludağ K, Dubowitz D, Yoder E, Restom K, Liu T and Buxton R 2004 Coupling of cerebral blood flow and oxygen consumption during physiological activation and deactivation measured with fMRI *NeuroImage* **23** 148–55

Vignal C, Boumans T, Montcel B, Ramstein S, Verhoye M, Van Audekerke J, Mathevon N, Van der Linden A and Mottin S 2008 Measuring brain hemodynamic changes in a songbird: response to hypercapnia measured with functional MRI and near-infrared spectroscopy *Phys. Med. Biol.* **53** 2457–70

Witt S, Laird A and Meyerand M 2008 Functional neuroimaging correlates of finger-tapping task variations: an ALE meta-analysis *NeuroImage* **42** 343–56

Worsley K J and Friston K J 1995 Analysis of fMRI time-series revisited-again *NeuroImage* **2** 173–81
Wu G, Luo F, Li Z, Zhao X and Li S 2002 Transient relationships among BOLD, CBV, and CBF changes in rat brain as detected by functional MRI *Magn. Reson. Med.* **48** 987–93
Ye J, Tak S, Jang K, Jung J and Jang J 2009 NIRS-SPM: statistical parametric mapping for near-infrared spectroscopy *NeuroImage* **44** 428–47
Zheng Y and Mayhew J 2009 A time-invariant visco-elastic windkessel model relating blood flow and blood volume *NeuroImage* **47** 1371–80